Journal of Cleaner Production 190 (2018) 443–451

Contents lists available at ScienceDirect

Journal of Cleaner Production

journal homepage: www.elsevier.com/locate/jclepro

Removal of nickel ions from aqueous solutions by manganese dioxide derived from groundwater treatment sludge

Dennis C. Ong [a, b], Sheila Mae B. Pingul-Ong [a, b], Chi-Chuan Kan [c, *], Mark Daniel G. de Luna [b, d, **]

[a] School of Technology, University of the Philippines Visayas, Miagao, Iloilo 5023, Philippines
[b] Environmental Engineering Program, National Graduate School of Engineering, University of the Philippines, Diliman, Quezon City 1101, Philippines
[c] Institute of Hot Spring Industry, Chia-Nan University of Pharmacy and Science, Tainan 71710, Taiwan, ROC
[d] Department of Chemical Engineering, University of the Philippines, Diliman, Quezon City 1101, Philippines

ARTICLE INFO

Article history:
Received 2 December 2017
Received in revised form
17 April 2018
Accepted 18 April 2018
Available online 21 April 2018

Keywords:
Adsorption
Groundwater treatment sludge
Heavy metals
Isotherm adsorption models
Wastewater treatment

ABSTRACT

In this study, manganese dioxide (MnO_2) derived from groundwater treatment sludge was used in the adsorption of nickel (Ni(II)) ions from aqueous solutions. The synthetic MnO_2 was prepared via permanganate reduction using manganese extracted from the sludge by reductive acid leaching and hydroxide precipitation. Scanning electron microscopy images showed aggregated micron-sized MnO_2 particles. Fourier transform infrared analysis of MnO_2 revealed functional groups at 3,396 cm^{-1}, 1,630 cm^{-1}, 1,427 cm^{-1} and 468 cm^{-1} bands. Zeta potential measurements at the pH range of 2–8 confirmed the net negative surface charge of MnO_2 particles. Moreover, Ni(II) adsorption by MnO_2 was best described by the Langmuir isotherm model, as indicated by the high values for the coefficients of determination ($R^2 > 0.9703$). The separation factor (R_L) for the range of pH values and initial Ni(II) concentrations considered in this study indicated that Ni(II) adsorption by MnO_2 was favorable. The kinetic data of Ni(II) adsorption by MnO_2 at pH 6.5 and initial Ni(II) concentrations from 10 to 200 mg L^{-1} conformed to the pseudo-second order adsorption kinetic model, with $R^2 > 0.9997$. Chemisorption occurred through the complexation of Ni(II) ions with available MnO_2 functional groups. The thermodynamic study at temperatures of 298.15, 308.15 and 318.15 K revealed that Ni(II) adsorption by MnO_2 was spontaneous and thermodynamically favorable for initial Ni(II) concentrations ranging from 50 to 200 mg L^{-1}. Overall, Ni(II) adsorption by MnO_2 was endothermic, as indicated by the positive ΔH° values. In addition, MnO_2 had good affinity towards the Ni(II) ions, as shown by the positive ΔS° values at all Ni(II) concentrations. Simple cost analysis revealed that the MnO_2 production from groundwater sludge was economically viable and may be scaled up for commercial applications.

1. Introduction

The electroplating industry is one of the significant contributors of water pollution due to the heavy metal species in its high volume rinse water (Almazán-Ruiz et al., 2015). Nickel is one of the toxic and hazardous heavy metals found in rinse waters at concentrations ranging from 900 to 1,583 ppm (Sulaiman and Othman, 2017). Its removal from contaminated waters is of extreme importance in order to prevent nickel-induced diseases and abnormalities, such as birth defects, embolism, chronic bronchitis, anemia, diarrhea, encephalopathy, hepatitis, lung and kidney damage, gastrointestinal distress, pulmonary fibrosis, renal edema, skin dermatitis, and central nervous system dysfunction (Futalan et al., 2011; Zhang and Wang, 2015). Nickel and other heavy metals can be removed from contaminated waters by chemical separation, membrane processes, electro-chemical treatment, electro-deposition and adsorption (Ghaee et al., 2012). However, most of these metal separation strategies are expensive and ineffective in treating wastewaters with low concentrations of heavy metal pollutants (Mangaleshwaran et al., 2015). In such cases, adsorption has several advantages, including lower cost, easier operation, and higher

* Corresponding author. Institute of Hot Spring Industry, Chia-Nan University of Pharmacy and Science, Tainan 71710, Taiwan, ROC.
** Corresponding author. Department of Chemical Engineering, University of the Philippines, Diliman, Quezon City 1101, Philippines..
E-mail addresses: cckanev@mail.cnu.edu.tw (C.-C. Kan), mgdeluna@up.edu.ph (M.D.G. de Luna).

https://doi.org/10.1016/j.jclepro.2018.04.175
0959-6526/

efficiency compared to other technologies (Xu et al., 2016). Some of the adsorbents used in nickel removal from wastewaters include activated carbon and biochar (Higashikawa et al., 2016; Pap et al., 2017), non-conventional low-cost materials, nanomaterials, composites and nanocomposites (Raval et al., 2016).

Manganese dioxide has high potential for heavy metals removal from aqueous media via adsorption. The utilization of manganese dioxide, or compounds containing manganese dioxide, as heavy metal adsorbent has been explored in previous studies. For example, δ-MnO_2 with magnetic properties has been used for the removal of Cd(II), Ni(II) and Pb(II) ions from aqueous solution (Calderon Rosas et al., 2010); nanosized hydrous manganese dioxide (HMO) impregnated onto a porous polystyrene cation exchanger resin for enhanced lead removal (Su et al., 2009); manganese oxide-coated sand (MOCS) for removing Cu(II) and Pb(II) (Han et al., 2006); hydrous manganese dioxide-poly (N-hydroxymethyl acrylamide/2-hydroxyethyl acrylate) (HMO-P(HMAm/HEA)) hydrogel to effectively remove Pb(II), Cu(II), Cd(II) and Ni(II) from water (Zhu and Li, 2015); manganese dioxide for sorption of As(III) and As(V) (Ajith et al., 2013), and α- and δ-phase manganese dioxide nanoadsorbents for arsenate adsorption (Singh et al., 2010).

Manganese dioxide can be obtained from various sources. Some types are naturally-occurring and can be found in marine sediments (Schippers and Jorgensen, 2001), or extracted from mine ores (Devi et al., 2000). Other types are synthetic and can be prepared as colloidal particles (Altaf et al., 2009), or doped on other materials such as silica gel (Varma et al., 1997) or titanium dioxide (Villaseñor et al., 2002). In the studies conducted on the synthesis of manganese dioxide, the manganese was obtained from commercially-available reagents, such as potassium permanganate and manganese sulfate. Among these are water-soluble colloidal MnO_2 (Perez-Benito and Arias, 1992) and in-situ formed MnO_2 (Qin et al., 2011). There are, however, other sources of manganese that have not been explored. In particular, groundwater treatment sludge contains significant amount of manganese that may be recovered and used for other purposes such as pollution prevention.

Recovery of manganese from groundwater treatment sludge can add value to the solid waste material. This insoluble product of groundwater oxidation contains high concentrations of manganese and iron precipitates, and are formed by aeration or by application of chemical oxidants, such as chlorine, hypochlorite, chlorine dioxide, ozone or potassium permanganate (Kan et al., 2012). Current disposal options for this solid waste are not sustainable and do not consider extraction of these heavy metal components (Razali et al., 2007; Vaezi and Batebi, 2001).

Reductive leaching, which makes use of strong acid and reducing agent, is a potential process that can be applied to the groundwater treatment sludge to recover its manganese content. This process has already been explored in the extraction of manganese from mine ores (Nayl et al., 2011). Various acids and reductants have been considered in previous studies, such as sulfuric acid and sawdust (Hariprasad et al., 2007), nitric acid and molasses (Lasheen et al., 2009), sulfuric acid and methanol (Momade and Momade, 1999), sulfuric acid and cane molasses (Su et al., 2008), sulfuric acid and glucose (Trifoni et al., 2001), and sulfuric acid and hydrogen peroxide (Jiang et al., 2003).

In this study, manganese dioxide was synthesized using manganese derived from groundwater treatment sludge. This process involved reductive leaching of the manganese from the sludge using sulfuric acid and hydrogen peroxide, purification of the manganese sulfate by precipitation of the iron content, and synthesis of the manganese dioxide by permanganate reduction. To date, groundwater treatment sludge has not yet been considered as secondary source of manganese, and no study has reported on the application of reductive leaching and hydroxide precipitation processes for the recovery of the manganese from the sludge. The purpose of the present research is to investigate the potential of groundwater treatment sludge as source of manganese for the synthesis of manganese dioxide for the specific application of nickel removal from contaminated solutions.

2. Materials and methods

2.1. Chemicals

All solutions were prepared using analytical grade chemicals. Deionized water (18.2 MΩ-cm) for the preparation of solutions was obtained with Purelab Ultra by ELGA LabWater (UK). EMSURE® sulfuric acid from Merck (Germany), with a concentration of 95–97%, and hydrogen peroxide from Shimakyu's Pure Chemicals (Osaka, Japan), with a concentration of 35%, were used to prepare the solutions required in the reductive leaching. Riedel-de Haën potassium hydroxide pellets from Sigma-Aldrich (Czech Republic) with 85% purity was used to prepare the solutions required in the precipitation of metals for the recovery of manganese. Potassium permanganate from J.T. Baker (USA) with 99% purity was used in the synthesis of manganese dioxide. Merck Uvasol® Potassium Bromide for IR spectroscopy (Darmstadt, Germany) was used for the FTIR spectroscopy analysis of the solid products after manganese dioxide synthesis. EMSURE® fuming hydrochloric acid, from Merck (Germany), with a concentration of 37%, and Riedel-de Haën potassium hydroxide pellets from Sigma-Aldrich (Czech Republic), with 85% purity, were used to prepare the solutions required in the pH adjustment for the analysis of the zeta potential of the MnO_2 sample, as well as in the adsorption experiments. Nickel (II) nitrate from Ferak. Laborat GmbH (Germany), with 97% purity, was used to prepare the solutions for the adsorption experiments.

2.2. Manganese dioxide synthesis

The groundwater treatment sludge used in the manganese dioxide synthesis was obtained from Changhua Water Treatment Plant located in central Taiwan. The sludge was dried in a Memmert UFE 400 laboratory oven (Germany) for 24 h at 105 °C to remove the moisture. Reductive leaching experiments were carried out in a 125-mL glass stoppered Duran Erlenmeyer flask placed on a PC-420D stirring hot plate by Corning, Inc. (USA). Dried sludge (3 g) was leached using 50 mL of 0.3 mol L^{-1} sulfuric acid and 5 mL of 0.8 mol L^{-1} hydrogen peroxide. The leaching process was conducted at 5 min leaching time, 150 rpm agitation rate and 25 °C operating temperature. Temperature adjustment of the aqueous sulfuric acid solution was first carried out in the flask. The dried sludge sample was added to the agitated aqueous sulfuric acid solution at the required temperature. Leaching started after hydrogen peroxide was added to the solution. After the leaching process, the slurry was filtered using Whatman 40 ashless filter paper from GE Healthcare (UK) with nominal particle retention of 8 μm. Manganese recovery was carried out in a 50-mL Pyrex beaker by precipitating the iron in the leachate using 0.4 mol L^{-1} KOH. The KOH solution was added dropwise into the agitated leachate until the pH 4.0 was achieved. EZ-DO 6011 waterproof pH tester by G&B (Taiwan) was used to measure the pH of solutions. At the end of the precipitation process, the slurry was filtered using Whatman 40. The filtrate from the precipitation process was stirred continuously while adding stoichiometric amount of $KMnO_4$ solution drop-wise to produce manganese dioxide, according to Eq. (1) (Qin et al.,

2011):

$$3MnSO_4 + 2KMnO_4 + 2H_2O \rightarrow 5MnO_2 + K_2SO_4 + 2H_2SO_4 \quad (1)$$

The resulting manganese dioxide was washed with distilled water until the pH of the filtrate was neutral.

2.3. Analytical methods

The solid samples after synthesis were placed on the top of a stub and coated with gold for 120 s in the E−1010 ion sputter coater (Hitachi Ltd., Japan). The coated samples were then mounted in the Hitachi S-3000N scanning electron microscope (Japan) for imaging. Images at 10,000× magnification were recorded. Samples of the sludge and synthetic MnO_2 were mixed with potassium bromide powder and pressed into a translucent disk. The prepared samples were analyzed in the JASCO FTIR 410 spectrometer in the 400–4000 cm^{-1} range. The synthetic MnO_2 were mixed with deionized water for zeta potential analysis. Samples for different pH levels were prepared by adjusting the sample pH with 0.1 M HCl or 0.1 M KOH. Afterwards, the samples were poured into a cuvette and mounted into the Brookhaven ZetaPlus (USA) for analysis. The profile of the zeta potential at different pH levels was plotted. Perkin Elmer (Australia) Optima 2000 DV inductively coupled plasma optical emission spectrometer (ICP-OES) was used in the analysis of the nickel content of the filtrates after adsorption experiments.

2.4. Adsorption studies

The adsorption experiments were carried out in a 125-mL Duran Erlenmeyer flask with glass stopper. The samples were agitated in the reciprocal shaker bath (BT-350, YIH, Taiwan) at specified duration. After each run, the samples were filtered, and the final nickel content of the filtrate was analyzed. The effect of solution pH and initial concentration on nickel adsorption was determined by mixing 10 g L^{-1} of MnO_2 with 25 mL of nickel solution for 120 min at an agitation rate of 50 rpm and temperature of 25 °C. The nickel solutions used had initial concentrations of 10, 50, 100 and 200 mg L^{-1}. The initial pH of the solutions were adjusted to 4.5, 5.5, 6.5 and 7.5 by addition of 0.1 N HNO_3 or 0.1 N KOH.

The adsorption isotherm of nickel on the manganese dioxide was determined by mixing 10 g L^{-1} of MnO_2 with 25 mL of nickel solution at an agitation rate of 50 rpm and temperature of 25 °C. The initial nickel concentrations were 10, 50, 100 and 200 mg L^{-1} and the initial pH of the solutions were adjusted to 4.5, 5.5, 6.5 and 7.5 by addition of 0.1 N HNO_3 or 0.1 N KOH. The adsorption kinetics of nickel on the manganese dioxide was determined by mixing 10 g L^{-1} of MnO_2 with 25 mL of nickel solution at agitation rate of 50 rpm and temperature of 25 °C. Solutions were in contact with the adsorbents for the duration of 10, 30, 60, 120, 360, 720 and 1440 min. The initial nickel concentrations were 10, 50, 100 and 200 mg L^{-1} and the initial pH of the solutions were adjusted to 6.5 by addition of 0.1 N HNO_3 or 0.1 N KOH. The adsorption thermodynamics of nickel on the manganese dioxide was determined by mixing 10 g L^{-1} of MnO_2 with 25 mL of nickel solution at pH 6.5, agitation rate of 50 rpm and initial nickel concentrations of 10, 50, 100 and 200 mg L^{-1}. The temperatures of the solutions were varied at 298.15, 308.15 and 318.15 K.

3. Results and discussion

3.1. Characterization of manganese dioxide

As shown in Fig. 1a, the synthetic manganese particles appear as clusters or clumps, thereby confirming the results of a previous study (Han et al., 2006). These aggregates of micron-sized porous

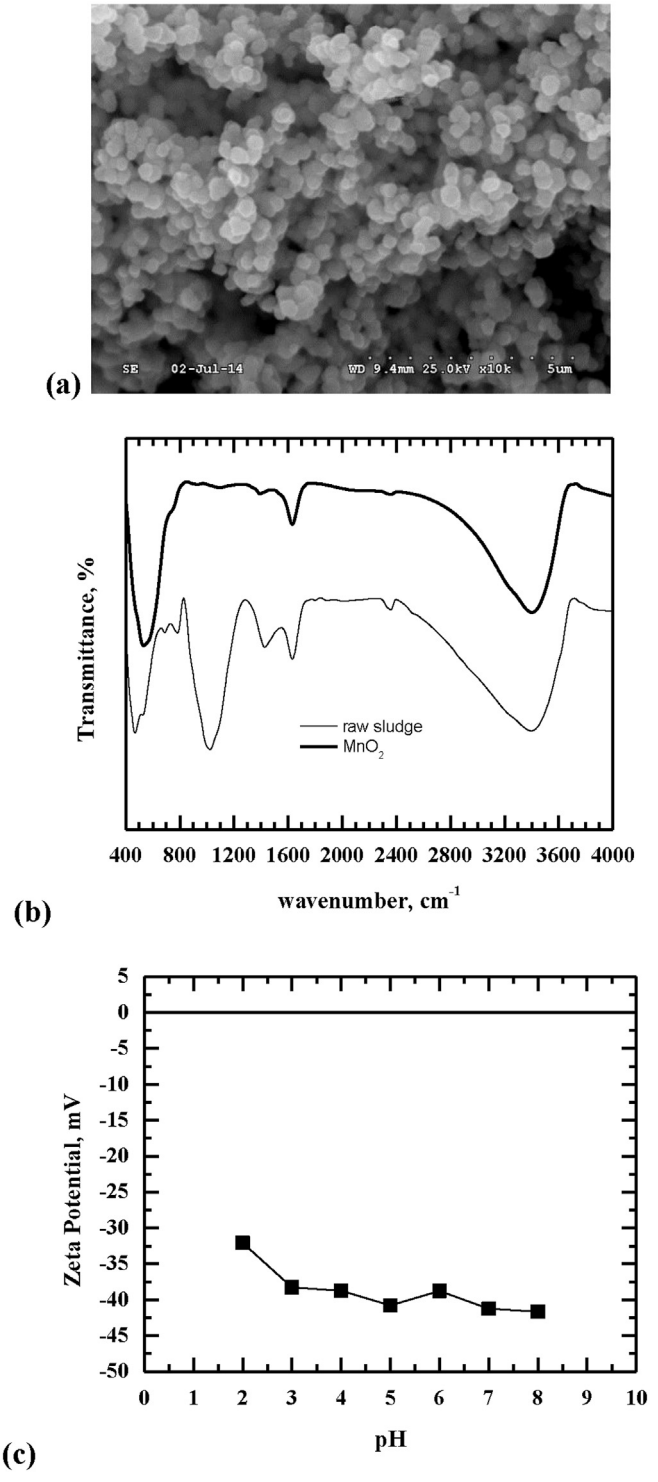

Fig. 1. **(a)** SEM micrograph of synthetic MnO_2 at 10,000× magnification, **(b)** FTIR spectra of groundwater treatment sludge and synthetic MnO_2 and **(c)** zeta potential of the synthetic MnO_2.

particles in Fig. 1a suggest that the manganese species are present in the oxide form (Ociński et al., 2016). Furthermore, the manganese dioxide obtained from the reaction of dilute $MnSO_4$ and dilute $KMnO_4$ solutions is in α-MnO_2 form, as reported by Fernandes et al. (1985). The characteristics observed in Fig. 1a are similar to the small spherical grains seen in the surface morphology of α-MnO_2 observed by Walanda et al. (2005).

Fig. 1b shows the results of the FTIR analysis of groundwater treatment sludge and the synthetic MnO_2. Previous studies have reported on the presence of MnO_2 in the solid waste (Ociński et al., 2016; Ong et al., 2017). As shown in Fig. 1b, the contribution of MnO_2 in the available functional groups of the sludge is seen in the bands at 3,396 cm^{-1}, 1,630 cm^{-1}, 1,427 cm^{-1} and 468 cm^{-1}. The medium band at 3,396 cm^{-1} range corresponds to the stretching vibration of the hydroxyl groups (Kan et al., 2017; Siswoyo et al., 2014) or water molecules (Ociński et al., 2016) in both the sludge and MnO_2. The weak band at 1,630 cm^{-1} corresponds to the O-H bending vibration of adsorbed water molecules in the sludge and MnO_2 (Kan et al., 2017; Ociński et al., 2016). The weak band at 1,427 cm^{-1} is attributed to oxides present in the sludge and MnO_2 (Kan et al., 2017). The medium band at 468 cm^{-1} is associated to Mn-O stretching vibrations (Kan et al., 2017; Ociński et al., 2016).

As shown in Fig. 1c, negative zeta potential values were obtained at the selected pH range of 2–8. This implies that the sludge particles tend to be negatively-charged at low pH (de Luna et al., 2017). The observed net surface charge of the MnO_2 can be attributed to the tendency of the freshly precipitated metal oxides to bind with water molecules to form hydrated metal compounds (Manahan, 2004). This is followed by the loss of H^+ from the bound H_2O, thereby resulting in a negatively-charged colloidal metal compound. The zeta potential trend also denotes that the synthetic MnO_2 has potential for adsorption of positively-charged heavy metal cations like nickel even at low pH. The contribution of the net negative surface charge of MnO_2 present in compounds like groundwater treatment sludge in adsorption at pH below neutral level was previously reported (Ong et al., 2017).

3.2. Effect of solution pH and initial Ni(II) concentration on Ni(II) uptake

Fig. 2a shows the effects of solution pH and initial Ni(II) concentration on Ni(II) uptake by the synthesized MnO_2. At low initial metal concentration of 10 mg L^{-1}, the amount of Ni(II) adsorbed per unit mass of MnO_2 was constant at 24.93 mg g^{-1} for all pH levels. In this case, all Ni(II) ions were removed from the solution. At this Ni(II) concentration, the functional groups that served as binding sites for Ni(II) adsorption were still available, and pH was not a significant factor in Ni(II) adsorption by MnO_2. At initial Ni(II) concentration of 50 mg L^{-1}, the metal uptake was observed to increase slightly from 66.19 mg g^{-1} at pH 4.5 to 73.39 mg g^{-1} at pH 7.5. A similar trend was observed at initial Ni(II) concentration of 100 mg L^{-1}, where metal uptake increased slightly from 109.13 mg g^{-1} at pH 4.5 to 109.90 mg g^{-1} at pH 7.5. At high initial Ni(II) concentration of 200 mg L^{-1}, it was observed that the metal uptake improved from 111.50 mg g^{-1} at pH 4.5 to 138.42 mg g^{-1} at pH 7.5. However, no statistically significant difference (ANOVA, $P > 0.05$) due to pH increase was found in the nickel uptake for any of the given initial Ni(II) concentration s considered. The effect of pH at all initial Ni(II) concentration levels was consistent with the data on the zeta potential of MnO_2 in Fig. 1c. At this pH range, the same amount of negatively-charged MnO_2 surface interacted with Ni(II) ions at each pH level and initial Ni(II) concentration (Ong et al., 2017).

In Fig. 2a, the Ni(II) uptake of the synthetic MnO_2 improved as the initial Ni(II) concentration was increased, regardless of solution pH. Fig. 2a suggests that lesser amount of Ni(II) ions competed for sorption on the MnO_2 when 10 mg L^{-1} of initial nickel concentration was used. The increase in the amount of Ni(II) ions present in

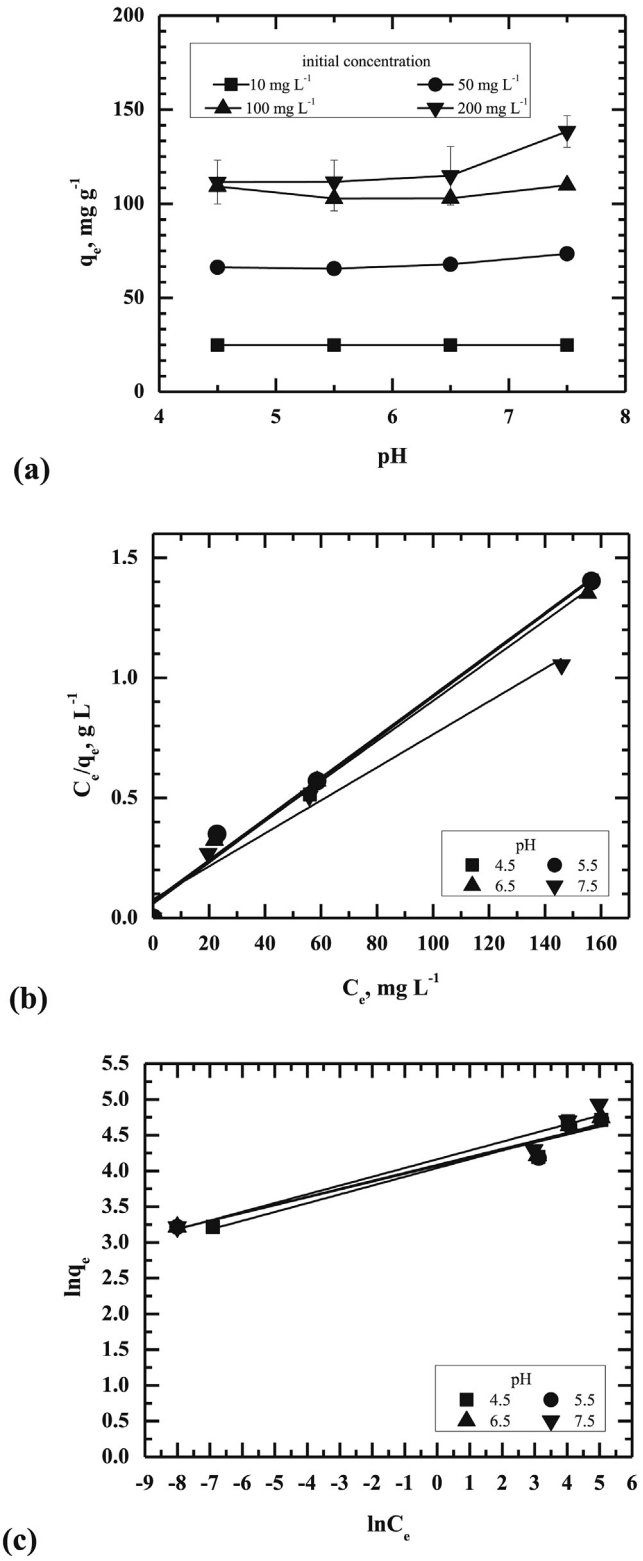

Fig. 2. **(a)** Effect of solution pH and initial Ni(II) concentration, **(b)** Langmuir and **(c)** Freundlich isotherm plots on the Ni(II) uptake by synthetic MnO_2.

the system increased the interaction through collision among Ni(II) ions and available adsorption sites on the adsorbent, resulting in increased metal uptake (de Luna et al., 2017). However, as more metal ions compete for the available adsorption sites, electrostatic repulsion between the metal ions bound on the adsorbent surface and the metal ions still present in the solution may occur (Zhang and Wang, 2015). This was observed in the smaller gain in Ni(II) uptake at higher initial metal concentrations (at concentrations of 100–200 mg L^{-1}), as seen in Fig. 2a.

3.3. Isotherm and kinetic studies

Adsorption isotherm experiments were conducted to elucidate the interactions between adsorbate molecules and the active sites on the adsorbent surface (Kara et al., 2017). Moreover, this provides a description on the amount of adsorbate that can be removed by a known quantity of adsorbent (de Luna et al., 2013). In this study, experimental data was fitted into adsorption isotherm models, namely Langmuir and Freundlich equations. The Langmuir isotherm describes monolayer adsorption (Langmuir, 1918) and assumes that a specific number of identical sites are homogeneously distributed over the adsorbent surface (Kara et al., 2017). Furthermore, it assumes that adsorption sites possess homogenous energy levels, no interactions occur between adsorbed molecules, and no transmigration of adsorbed molecules happen on the adsorption surface (de Luna et al., 2013). The Langmuir equation can be expressed by Eq. (2) and its linear form by Eq. (3):

$$q_e = \frac{q_{max} k_L C_e}{1 + k_L C_e} \tag{2}$$

$$\frac{C_e}{q_e} = \frac{1}{q_{max}} C_e + \frac{1}{k_L q_{max}} \tag{3}$$

where q_{max} (mg g^{-1}) is the maximum amount of metal ion per unit weight of sludge capable of forming complete monolayer coverage on the surface, bound at high equilibrium concentrations C_e; q_e is the amount of metal ion adsorbed per unit weight of sludge at equilibrium; k_L is the Langmuir adsorption constant related to the affinity of binding sites. A straight line for the plot of C_e/q_e versus C_e will give the q_{max} and k_L from the slope and intercept of the line, as shown in Fig. 2b.

The Freundlich isotherm describes adsorption on a heterogeneous surface with adsorption sites having varying energy levels (Freundlich, 1906). The model assumes that the stronger binding sites on a heterogeneous surface are occupied initially and that the binding strength falls with a rise in the degree of site occupation (de Luna et al., 2015). Furthermore, the Freundlich equation predicts that the amount of adsorbate on the sorbent will increase as long as there is an increase in the adsorbate concentration. The Freundlich equation is represented by Eq. (4) and its linear form by Eq. (5):

$$q_e = k_f C_e^{1/n} \tag{4}$$

$$ln q_e = ln k_f + \frac{1}{n} ln C_e \tag{5}$$

where k_f is roughly an indicator of the adsorption capacity and $1/n$ of the adsorption intensity. A straight line for the plot of $\ln q_e$ versus $ln C_e$ will yield the constant n and k_f from the slope and intercept of the line, as shown in Fig. 2c.

Table 1 presents a summary of the calculated adsorption parameters and coefficients of determination (R^2) for the two isotherm models by linear regression. Results show that the adsorption data had better fit with the Langmuir model, as reflected in the higher R^2 values obtained for the Langmuir model (0.9703–0.9847), compared with the Freundlich model (0.9172–0.9339). This implies that the experimental data of Ni(II) adsorption on MnO_2 could be best described by the Langmuir model. This is different from the trend observed for the groundwater treatment sludge, which had better fit with the Freundlich model (Ong et al., 2017). However, this is expected since the source sludge was composed of various components with different properties. The adsorption capacities calculated from the Langmuir model were in agreement with the experimental adsorption capacities at equilibrium for all pH values, as shown in Table 1. A dimensionless separation factor, R_L, based on the Langmuir model was used to evaluate the effectiveness of adsorption (Genuino et al., 2018). The value of R_L was calculated from the Langmuir constant, k_L, and initial concentration, C_0 (mg L^{-1}), according to Eq. (6):

Table 1
Isotherm parameters for Ni(II) adsorption by MnO_2.

Isotherm parameter	pH			
	4.5	5.5	6.5	7.5
q_{exp} (mg g^{-1})	111.50	111.67	114.92	138.42
Langmuir model				
q_{max} (mg g^{-1})	116.01	116.55	119.76	145.56
k_L (L mg^{-1})	0.1482	0.1232	0.1215	0.0888
R^2	0.9833	0.9832	0.9847	0.9703
Freundlich model				
k_f (mg g^{-1})/(mg L^{-1})	56.88	58.55	59.46	64.30
n	8.1327	9.1050	8.9518	8.1673
R^2	0.9172	0.9197	0.9339	0.9292

$$R_L = \frac{1}{1 + k_L C_0} \tag{6}$$

to determine if the adsorption is unfavorable ($R_L > 1$), linear ($R_L = 1$), favorable ($0 < R_L < 1$), or irreversible ($R_L = 0$) (Futalan et al., 2011). The computed R_L values for the initial concentration range of 10–200 mg L^{-1} at pH 4.5 (0.4029–0.0326), 5.5 (0.4480–0.0390), 6.5 (0.4515–0.0395) and 7.5 (0.5297–0.0533) suggest that adsorption was favorable. Thus, the synthetic MnO_2 is a suitable adsorbent for nickel ions. Furthermore, the adsorption capacity values obtained were higher than most adsorbents explored for nickel adsorption (Raval et al., 2016).

The effect of varying contact time on nickel adsorption capacity of MnO_2 at pH 6.5 and different initial nickel concentrations is presented in Fig. 3a. As shown, Ni(II) removal was fast during the early part of the adsorption process for all initial Ni(II) concentrations considered. These trends may be attributed to the abundance of the functional groups present on the MnO_2 surface that were available for binding with the Ni(II) ions. At this period, the electrostatic attraction between the negatively-charged MnO_2 and the positively-charged Ni(II) ions caused the rapid migration of the metal ions from the solution onto the surface of the adsorbent at a short period of time (Ong et al., 2017). At the latter part of the adsorption process, Ni(II) removal slowed down until equilibrium was reached. At this period, the functional groups on the MnO_2 became saturated with the Ni(II) ions. This caused electrostatic repulsion between the Ni(II) ions bound on the adsorbent surface and the Ni(II) ions remaining in the solution that prevented further adsorption of the metal ions onto the MnO_2 (Zhang and Wang, 2015).

Kinetics experiment is conducted to examine the mechanism that governs the adsorption of adsorbate onto the adsorbent

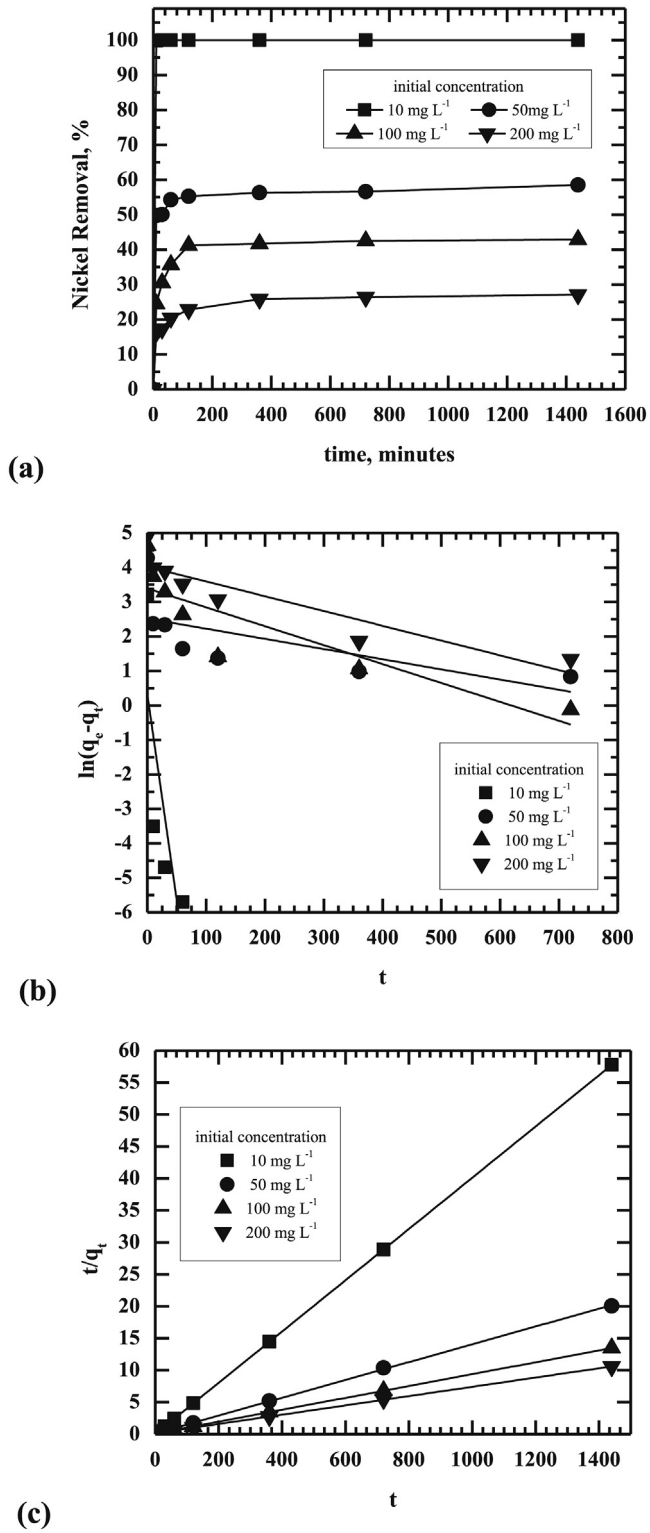

Fig. 3. **(a)** Effect of contact time, **(b)** pseudo-first order, and **(c)** pseudo-second order kinetic plots of Ni(II) uptake by MnO_2 at pH 6.5, 25 °C and varying initial Ni(II) concentration.

surface (de Luna et al., 2013). This is important in describing the rate-determining step of the adsorption process (Kan et al., 2017). In this study, pseudo-first order and pseudo-second order kinetics were considered in evaluating the experimental data. The pseudo-first order kinetic model, also known as the Lagergren equation (Lagergren, 1898), assumes that the rate-limiting mechanism of the adsorption process is physical adsorption. The linearized kinetic rate equation can be written as Eq. (7) for the pseudo-first order model:

$$ln(q_e - q_t) = lnq_e - k_1 t \quad (7)$$

where k_1 is the rate constant of pseudo-first order adsorption (min^{-1}); q_e and q_t are the amount of metal ion adsorbed per gram of sludge (mg g^{-1}) at equilibrium and at any time, t, respectively. A straight line for the plot of ln (q_e - q_t) versus t would give the first-order rate constant k_1 and equilibrium adsorption capacity q_e, from the slope and intercept of the line, as shown in Fig. 3b.

The pseudo-second order kinetic model (Ho and McKay, 1998) assumes that the rate-limiting mechanism of the adsorption process is chemisorption. The linearized kinetic rate equation can be written as Eq. (8) for the pseudo-second order kinetics:

$$\frac{t}{q_t} = \frac{1}{k_2 q_e^2} + \frac{t}{q_e} \quad (8)$$

where k_2 (g mg^{-1} min^{-1}) is the rate constant of pseudo-second order adsorption. The plot of t/q_t versus t would give the pseudo-second order rate constants k_2 and q_e, as shown in Fig. 3c.

Table 2 presents the obtained kinetic model parameters and coefficients of determination (R^2) by linear regressions using the two kinetic models. The kinetic data of nickel adsorption at pH 6.5 and varying initial Ni(II) concentrations of 10, 50, 100 and 200 mg L^{-1} was fitted to pseudo-first order and pseudo-second order models. Results show that pseudo-second order kinetic model had higher R^2 values at 0.9997 to 0.9999, as compared with that of pseudo-first order kinetic model at 0.3331 to 0.7958. Furthermore, as shown in Table 2, the calculated adsorption capacities from the pseudo-second order kinetic model were in agreement with the experimental adsorption capacities at equilibrium. This implies that the kinetic data may be best described by the pseudo-second order adsorption kinetic rate model. As such, the rate-limiting step for the Ni(II) sorption onto the MnO_2 can be attributed to chemical adsorption where there is formation of covalent bond through the exchange or sharing of electrons between the metal ions and the binding sites of the adsorbent (de Luna et al., 2018). This occurred through complexation of the Ni(II) ions with the available functional groups on the MnO_2. Highest value of the pseudo-second order rate constant, k_2, was obtained at the low initial Ni(II) concentration of 10 mg L^{-1}. This signifies the less competition between metal ions in binding to the functional groups at low Ni(II) concentrations. As a result, the Ni(II) ions were quickly adsorbed by MnO_2.

Table 2
Kinetic model parameters for Ni(II) adsorption by MnO_2.

Kinetic parameter	Initial nickel concentration (mg L^{-1})			
	10	50	100	200
q_{exp} (mg g^{-1})	24.93	71.76	106.95	136.42
Pseudo-first-order model				
q_e (mg g^{-1})	1.37	12.44	29.79	55.95
k_1 (min^{-1})	0.11947	0.00295	0.00548	0.00429
R^2	0.4245	0.3331	0.7166	0.7958
Pseudo-second-order model				
q_e (mg g^{-1})	24.93	71.68	107.64	137.74
k_2 (g $mg^{-1}min^{-1}$)	5.66	0.0018	0.0009	0.0004
R^2	0.9999	0.9997	0.9999	0.9998

3.4. Thermodynamic study and cost estimation of MnO_2 production

Fig. 4a presents the effect of varying temperature on the adsorption of Ni(II) ions at pH 6.5 by the synthetic MnO_2. It was observed that at the low initial Ni(II) concentration of 10 mg L^{-1} (not shown), all Ni(II) ions were removed from the aqueous solution and the metal uptake was constant at 24.93 mg g^{-1} for all temperature levels. This implies that at this low concentration, temperature was not a significant factor in the Ni(II) uptake of the given amount of MnO_2 used in the experiment. As shown in Fig. 4a, increasing trends in Ni(II) uptake was observed as the temperature was increased for the initial Ni(II) concentrations above 10 mg L^{-1}. For the increase in temperature from 298.15 to 318.15 K, the Ni(II) uptake increased from 68 to 86 mg g^{-1}, 103–160 mg g^{-1}, and 115–283 mg g^{-1} for the initial metal concentrations of 50, 100 and 200 mg L^{-1}, respectively. This suggests that at higher initial metal concentrations, temperature had a significant effect on the Ni(II) uptake of the MnO_2. The observed trends imply that the adsorption process was endothermic, where the net heat was absorbed during the adsorption process (Saman et al., 2016). This energy present in the system at higher temperatures facilitated the binding of Ni(II) ions to the surface of the MnO_2 (Zhang and Wang, 2015).

To further understand the thermodynamics of adsorption, the Gibbs free energy change (ΔG°), enthalpy change (ΔH°), and entropy change (ΔS°) were calculated using Eq. (9) and Eq. (10) to determine the spontaneity, thermal feasibility and nature of the reaction (Chen et al., 2016):

$$\Delta G^\circ = \Delta H^\circ - T\Delta S^\circ \tag{9}$$

$$lnK_c = -\frac{\Delta H^\circ}{RT} + \frac{\Delta S^\circ}{R} \tag{10}$$

where K_C is the ratio between the amount of nickel that is adsorbed at equilibrium (mg L^{-1}) and C_e is the equilibrium concentration of nickel (mg L^{-1}), R is the universal gas constant 8.314 (J mol^{-1} K^{-1}) and T is the absolute temperature (K). ΔH° and ΔS° are obtained from the slope and intercept of a plot of ln K_C versus 1/T, as shown in Fig. 4b. Table 3 summarizes the thermodynamic parameters of the Ni(II) adsorption by MnO_2. At all initial concentrations considered, the ΔG° had a negative sign at all temperature levels. This implies that the adsorption was spontaneous and thermodynamically favorable for the selected conditions (Lǔ et al., 2013). Furthermore, the magnitude of ΔG° increased with temperature, which implies an increased degree of spontaneity at high temperature and resulted in increase in adsorption capacity (Saman et al., 2016). The ΔH° at all Ni(II) concentrations was positive, which implies that the adsorption process was endothermic in nature (Choi et al., 2017). In endothermic adsorption, the magnitude of the total energy absorbed by the system due to bond breaking is greater than the magnitude of the total energy released due to bond making (Kan et al., 2013). The bond breaking energy may be attributed to the displacement of previously adsorbed H^+ from the surface of the MnO_2, while the bond making energy may be associated with the formation of activated complex and the final sorption of Ni(II) ions onto the adsorbent surface. Furthermore, the ΔS° at all Ni(II) concentrations was positive, which suggests that the randomness of the solid-solution interface has increased and indicates a good affinity of nickel ions towards MnO_2 (Futalan et al., 2011).

Table 4 presents the results of previous studies on the utilization of various adsorbents for nickel removal, in comparison with the results of the present research. As shown, the isotherm, kinetics and thermodynamic findings of the present study were consistent with those from published results. Furthermore, the adsorption capacity of the sludge-derived MnO_2 was higher than the reported values on nickel removal from previous studies.

An estimate of the production cost of manganese dioxide by reductive leaching, hydroxide precipitation and permanganate reduction methods is summarized in Table 5. A simple evaluation of the economic feasibility of MnO_2 production will give an indicator of its profitability in commercial applications (Lam et al., 2017). As shown in Table 5, the estimation was based on the cost incurred by the procurement and transportation of groundwater treatment sludge, chemicals, and utilities (electricity) consumed during the production of MnO_2. The production cost was estimated to be about USD 151.67/kg of MnO_2, which is comparably lower than the

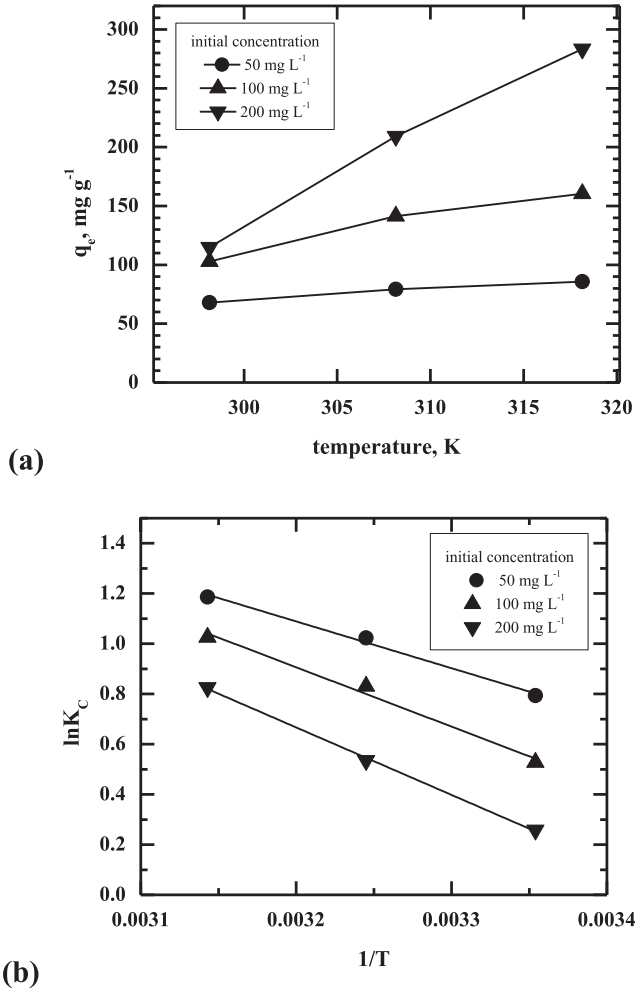

Fig. 4. **(a)** Effect of solution temperature on Ni(II) uptake by MnO_2 and **(b)** *lnKc* vs *1/T* plot at pH 6.5 and varying initial Ni(II) concentration.

Table 3
Thermodynamic parameters for Ni(II) adsorption by MnO_2 at pH 6.5.

Thermodynamic parameter	Temperature (K)	initial nickel concentration (mg L^{-1})		
		50	100	200
ΔG° (kJ mol^{-1})	298.15	−1.99	−1.34	−0.63
	308.15	−2.57	−2.05	−1.40
	318.15	−3.16	−2.75	−2.17
ΔH° (kJ mol^{-1})		15.49	19.65	22.34
ΔS° (J mol^{-1} K^{-1})		58.63	70.40	77.033

Table 4
Nickel adsorption properties of various adsorbents.

Adsorbent	q_{max} (mg g^{-1})	Isotherm study	Kinetics study	Thermodynamic study	pH	Adsorbent dosage	References
δ-MnO_2	30.63	Langmuir	PSO	Endothermic	8.0	–	(Ren et al., 2011)
Graphene nanosheet/δ-MnO_2 (GNS/MnO_2) composite	46.55	Langmuir	PSO	Endothermic	8.0	–	(Ren et al., 2011)
Biochar from chicken manure mixed with sawdust, sugarcane straw, rice husk, and sawdust	0.2 to 10.9	–	–	–	5.34 to 7.46	0.10 g/30 mL	(Higashikawa et al., 2016)
Activated carbon from plum stones	63.74	Freundlich	PSO	Exothermic	6.0	0.10 g/50 mL	(Pap et al., 2017)
Metakaolin based geopolymer	42.61	Langmuir	PSO	–	7.25	0.08 g/25 mL	(Kara et al., 2017)
Lignocellulose/montmorillonite (LNC/MMT) nanocomposite	94.86	Langmuir	PSO	–	6.8	0.10 g/50 mL	(Zhang and Wang, 2015)
Groundwater treatment sludge-derived MnO_2	138.42	Langmuir	PSO	Endothermic	6.5	0.01 g/25 mL	This study

PSO – pseudo second order.

Table 5
Estimated production cost (USD kg^{-1}) of the sludge-derived MnO_2.

Components	Estimated cost (USD kg^{-1})
Groundwater treatment sludge[a]	0
Transportation[b]	0.31
Chemicals	
Sulfuric acid	32.74
Hydrogen peroxide	10.34
Potassium hydroxide	24.28
Potassium permanganate	47.17
Deionized water	33.55
Electrical consumption[c]	
Sludge drying	3.25
Reductive leaching	0.01
Hydroxide precipitation	0.01
MnO_2 synthesis	0.01
Total estimated production cost	151.67
Commercial reagent-grade MnO_2	222.08

[a] Obtained free of charge.
[b] Based on USD 96.99 vehicle rent with 1500 kg loading capacity in the Philippines.
[c] Based on USD 0.17 per kWh charge rate of electricity in the Philippines.

market price of reagent-grade MnO_2 (USD 222.08/kg of MnO_2). This is a good indication that the synthesis of MnO_2 using manganese recovered from groundwater treatment sludge by reductive leaching, hydroxide precipitation and permananganate reduction is economically viable, and the MnO_2 production could be scaled-up for commercial applications. However, since this study was conducted in a laboratory scale, further improvement of the production method is needed, and may include exploring other acid medium and reducing agents for the synthesis of the adsorbent, as well as testing with higher initial nickel concentrations and reusability of the adsorbent.

4. Conclusions

This study demonstrated the potential of MnO_2 derived from groundwater treatment sludge for nickel removal from aqueous solutions. Nickel removal was best described by the Langmuir isotherm model, which suggests monolayer adsorption on the MnO_2. Chemisorption through complexation with the functional groups on MnO_2 governed the nickel adsorption process. The net negative surface charge of MnO_2 facilitated in the removal of Ni(II) ions at the pH range of 4.5–7.5. Adsorption was generally spontaneous and thermodynamically favorable. The adsorption process at all conditions was endothermic, and MnO_2 had good affinity towards the Ni(II) ions, as suggested by the positive ΔH° and ΔS° values. The MnO_2 production was found to be economically viable and has potential to be scaled up for commercial applications. The findings of the study revealed the potential of groundwater treatment sludge as an alternative source of manganese dioxide adsorbent for pollutant removal.

Declarations of interest

None.

Acknowledgement

The authors would like to thank the Ministry of Science and Technology, Taiwan (Contract No. MOST-102-2221-E-041-005) and the Department of Science and Technology, Philippines for providing financial support for this research undertaking.

References

Ajith, N., Dalvi, A., Swain, K.K., Devi, P.S.R., Kalekar, B.B., Verma, R., Reddy, A.V.R., 2013. Sorption of As(III) and As(V) on chemically synthesized manganese dioxide. J. Environ. Sci. Health. A. Tox. Hazard. Subst. Environ. Eng. 48, 422–428. https://doi.org/10.1080/10934529.2013.728919.
Almazán-Ruiz, F., Caballero, F., Cruz-Díaz, M., Rivero, E., Vazquez-Arenas, J., González, I., 2015. Nickel recovery from an electroplating rinsing effluent using RCE bench scale and RCE pilot plant reactors: the influence of pH control. Chem. Eng. Res. Des. 97, 18–27. https://doi.org/10.1016/j.cherd.2015.02.022.
Altaf, M., Akram, M., Kabir-ud-Din, 2009. Water-soluble colloidal manganese dioxide as an oxidant for l-tyrosine in the absence and presence of non-ionic surfactant TX-100. Colloids Surfaces B Biointerfaces 73, 308–314. https://doi.org/10.1016/j.colsurfb.2009.05.033.
Calderon Rosas, C.A., Franzreb, M., Valenzuela, F., Höll, W.H., 2010. Magnetic manganese dioxide as an amphoteric adsorbent for removal of harmful inorganic contaminants from water. React. Funct. Polym. 70, 516–520. https://doi.org/10.1016/j.reactfunctpolym.2010.03.011.
Chen, T.C., Sapitan, J.F.F., Ballesteros, F.C., Lu, M.C., 2016. Using activated clay for adsorption of sulfone compounds in diesel. J. Clean. Prod. 124, 378–382. https://doi.org/10.1016/j.jclepro.2016.03.004.
Choi, A.E.S., Roces, S., Dugos, N., Arcega, A., Wan, M.W., 2017. Adsorptive removal of dibenzothiophene sulfone from fuel oil using clay material adsorbents. J. Clean. Prod. 161, 267–276. https://doi.org/10.1016/j.jclepro.2017.05.072.
de Luna, M.D.G., Flores, E.D., Cenia, M.C.B., Lu, M.C., 2015. Removal of copper ions from aqueous solution by adlai shell (Coix lacryma-jobi L.) adsorbents. Bioresour. Technol. 192, 841–844. https://doi.org/10.1016/j.biortech.2015.06.018.
de Luna, M.D.G., Flores, E.D., Genuino, D.A.D., Futalan, C.M., Wan, M.W., 2013. Adsorption of Eriochrome Black T (EBT) dye using activated carbon prepared from waste rice hulls-Optimization, isotherm and kinetic studies. J. Taiwan Inst. Chem. Eng. 44, 646–653. https://doi.org/10.1016/j.jtice.2013.01.010.
de Luna, M.D.G., Murniati, Budianta, W., Rivera, K.K.P., Arazo, R.O., 2017. Removal of sodium diclofenac from aqueous solution by adsorbents derived from cocoa pod husks. J. Environ. Chem. Eng. 5, 1465–1474. https://doi.org/10.1016/j.jece.2017.02.018.
de Luna, M.D.G., Samaniego, M.L., Ong, D.C., Wan, M.-W., Lu, M.-C., 2018. Kinetics of sulfur removal in high shear mixing-assisted oxidative-adsorptive desulfurization of diesel. J. Clean. Prod. 178, 468–475. https://doi.org/10.1016/j.jclepro.2018.01.049.
Devi, N.B., Madhuchhanda, M., Rao, K.S., Rath, P.C., Paramguru, R.K., 2000. Oxidation of chalcopyrite in the presence of manganese dioxide in hydrochloric acid medium. Hydrometallurgy 57, 57–76. https://doi.org/10.1016/S0304-386X(00)00100-6.
Fernandes, J.B., Desai, B.D., Dalal, V.N.K., 1985. Manganese dioxide - a review of a battery chemical part I. Chemical syntheses and X-ray diffraction studies of manganese dioxides. J. Power Sources 15, 209–237. https://doi.org/10.1016/

0378-7753(85)80075-6.
Freundlich, H., 1906. Über die Adsorption in Lösungen. Z. Phys. Chem. 57, 385–470. https://doi.org/10.1007/s10853-014-8602-8.
Futalan, C.M., Kan, C.C., Dalida, M.L., Hsien, K.J., Pascua, C., Wan, M.W., 2011. Comparative and competitive adsorption of copper, lead, and nickel using chitosan immobilized on bentonite. Carbohydr. Polym. 83, 528–536. https://doi.org/10.1016/j.carbpol.2010.08.013.
Genuino, D.A.D., de Luna, M.D.G., Capareda, S.C., 2018. Improving the surface properties of municipal solid waste-derived pyrolysis biochar by chemical and thermal activation: optimization of process parameters and environmental application. Waste Manag. 72, 255–264. https://doi.org/10.1016/j.wasman.2017.11.038.
Ghaee, A., Shariaty-Niassar, M., Barzin, J., Zarghan, A., 2012. Adsorption of copper and nickel ions on macroporous chitosan membrane: equilibrium study. Appl. Surf. Sci. 258, 7732–7743. https://doi.org/10.1016/j.apsusc.2012.04.131.
Han, R., Zou, W., Zhang, Z., Shi, J., Yang, J., 2006. Removal of copper(II) and lead(II) from aqueous solution by manganese oxide coated sand. I. Characterization and kinetic study. J. Hazard Mater. 137, 384–395. https://doi.org/10.1016/j.jhazmat.2006.02.021.
Hariprasad, D., Dash, B., Ghosh, M.K., Anand, S., 2007. Leaching of manganese ores using sawdust as a reductant. Miner. Eng. 20, 1293–1295. https://doi.org/10.1016/j.mineng.2007.07.013.
Higashikawa, F.S., Conz, R.F., Colzato, M., Cerri, C.E.P., Alleoni, L.R.F., 2016. Effects of feedstock type and slow pyrolysis temperature in the production of biochars on the removal of cadmium and nickel from water. J. Clean. Prod. 137, 965–972. https://doi.org/10.1016/j.jclepro.2016.07.205.
Ho, Y.S., McKay, G., 1998. A comparison of chemisorption kinetic models applied to pollutant removal on various sorbents. Process Saf. Environ. Protect. 76, 332–340. https://doi.org/10.1205/095758298529696.
Jiang, T., Yang, Y., Huang, Z., Qiu, G., 2003. Simultaneous leaching of manganese and silver from manganese-silver ores at room temperature. Hydrometallurgy 69, 177–186. https://doi.org/10.1016/S0304-386X(03)00033-1.
Kan, C.-C., Aganon, M.C., Futalan, C.M., Dalida, M.L.P., 2013. Adsorption of Mn^{2+} from aqueous solution using Fe and Mn oxide-coated sand. J. Environ. Sci. 25, 1483–1491. https://doi.org/10.1016/S1001-0742(12)60188-0.
Kan, C.-C., Chen, W.-H., Wan, M.-W., Phatai, P., Wittayakun, J., Li, K.-F., 2012. The preliminary study of iron and manganese removal from groundwater by NaOCl oxidation and MF filtration. Sustain. Environ. Res. 22, 25–30.
Kan, C.-C., Ibe, A.H., Rivera, K.K.P., Arazo, R.O., de Luna, M.D.G., 2017. Hexavalent chromium removal from aqueous solution by adsorbents synthesized from groundwater treatment residuals. Sustain. Environ. Res. 27, 163–171. https://doi.org/10.1016/j.serj.2017.04.001.
Kara, İ., Yilmazer, D., Akar, S.T., 2017. Metakaolin based geopolymer as an effective adsorbent for adsorption of zinc(II) and nickel(II) ions from aqueous solutions. Appl. Clay Sci. 139, 54–63. https://doi.org/10.1016/j.clay.2017.01.008.
Lagergren, S., 1898. Zur theorie der sogenannten adsorption geloster stoffe (About the theory of so-called adsorption of soluble substances). K. Sven. Vetenskapsakademiens. Handlingar 24, 1–39.
Lam, S.S., Liew, R.K., Wong, Y.M., Yek, P.N.Y., Ma, N.L., Lee, C.L., Chase, H.A., 2017. Microwave-assisted pyrolysis with chemical activation, an innovative method to convert orange peel into activated carbon with improved properties as dye adsorbent. J. Clean. Prod. 162, 1376–1387. https://doi.org/10.1016/j.jclepro.2017.06.131.
Langmuir, I., 1918. The adsorption of gases on plane surfaces of glass, mica and platinum. J. Am. Chem. Soc. 40, 1361–1403. https://doi.org/10.1021/ja02242a004.
Lasheen, T.A., El-Hazek, M.N., Helal, A.S., El-Nagar, W., 2009. Recovery of manganese using molasses as reductant in nitric acid solution. Int. J. Miner. Process. 92, 109–114. https://doi.org/10.1016/j.minpro.2009.03.001.
Lǔ, J., Liu, H., Liu, R., Zhao, X., Sun, L., Qu, J., 2013. Adsorptive removal of phosphate by a nanostructured Fe-Al-Mn trimetal oxide adsorbent. Powder Technol. 233, 146–154. https://doi.org/10.1016/j.powtec.2012.08.024.
Manahan, S., 2004. Phase interactions. In: Environmental Chemistry. CRC Press, Boca Raton, FL, pp. 127–148.
Mangaleshwaran, L., Thirulogachandar, A., Rajasekar, V., Muthukumaran, C., Rasappan, K., 2015. Batch and fixed bed column studies on nickel (II) adsorption from aqueous solution by treated polyurethane foam. J. Taiwan Inst. Chem. Eng. 55, 112–118. https://doi.org/10.1016/j.jtice.2015.03.034.
Momade, F.W., Momade, Z., 1999. A study of the kinetics of reductive leaching of manganese oxide ore in aqueous methanol–sulphuric acid medium. Hydrometallurgy 54, 25–39. https://doi.org/10.1016/S0304-386X(99)00048-1.
Nayl, A.A., Ismail, I.M., Aly, H.F., 2011. Recovery of pure MnSO4·H2O by reductive leaching of manganese from pyrolusite ore by sulfuric acid and hydrogen peroxide. Int. J. Miner. Process. 100, 116–123. https://doi.org/10.1016/j.minpro.2011.05.003.
Ociński, D., Jacukowicz-Sobala, I., Mazur, P., Raczyk, J., Kociołek-Balawejder, E., 2016. Water treatment residuals containing iron and manganese oxides for arsenic removal from water - characterization of physicochemical properties and adsorption studies. Chem. Eng. J. 294, 210–221. https://doi.org/10.1016/j.cej.2016.02.111.
Ong, D.C., Kan, C.-C., Pingul-Ong, S.M.B., De Luna, M.D.G., 2017. Utilization of groundwater treatment plant (GWTP) sludge for nickel removal from aqueous solutions: isotherm and kinetic studies. J. Environ. Chem. Eng. 5, 5746–5753. https://doi.org/10.1016/j.jece.2017.10.046.
Pap, S., Šolević Knudsen, T., Radonić, J., Maletić, S., Igić, S.M., Turk Sekulić, M., 2017. Utilization of fruit processing industry waste as green activated carbon for the treatment of heavy metals and chlorophenols contaminated water. J. Clean. Prod. 162, 958–972. https://doi.org/10.1016/j.jclepro.2017.06.083.
Perez-Benito, J.F., Arias, C., 1992. A kinetic study of the reaction between soluble (colloidal) manganese dioxide and formic acid. J. Colloid Interface Sci. 149, 92–97. https://doi.org/10.1016/0021-9797(92)90394-2.
Qin, Q., Wang, Q., Fu, D., Ma, J., 2011. An efficient approach for Pb(II) and Cd(II) removal using manganese dioxide formed in situ. Chem. Eng. J. 172, 68–74. https://doi.org/10.1016/j.cej.2011.05.066.
Raval, N.P., Shah, P.U., Shah, N.K., 2016. Adsorptive removal of nickel(II) ions from aqueous environment: a review. J. Environ. Manag. 179, 1–20. https://doi.org/10.1016/j.jenvman.2016.04.045.
Razali, M., Zhao, Y.Q., Bruen, M., 2007. Effectiveness of a drinking-water treatment sludge in removing different phosphorus species from aqueous solution. Separ. Purif. Technol. 55, 300–306. https://doi.org/10.1016/j.seppur.2006.12.004.
Ren, Y., Yan, N., Wen, Q., Fan, Z., Wei, T., Zhang, M., Ma, J., 2011. Graphene/δ-MnO_2 composite as adsorbent for the removal of nickel ions from wastewater. Chem. Eng. J. 175, 1–7. https://doi.org/10.1016/j.cej.2010.08.010.
Saman, N., Johari, K., Song, S.T., Kong, H., Cheu, S.C., Mat, H., 2016. High removal efficiency of Hg(II) and MeHg(II) from aqueous solution by coconut pith - equilibrium, kinetic and mechanism analyses. J. Environ. Chem. Eng. 4, 2487–2499. https://doi.org/10.1016/j.jece.2016.04.033.
Schippers, A., Jorgensen, B.B., 2001. Oxidation of pyrite and iron sulfide by manganese dioxide in marine sediments. Geochim. Cosmochim. Acta 65, 915–922. https://doi.org/10.1016/S0016-7037(00)00589-5.
Singh, M., Thanh, D.N., Ulbrich, P., Strnadová, N., Štěpánek, F., 2010. Synthesis, characterization and study of arsenate adsorption from aqueous solution by α- and δ-phase manganese dioxide nanoadsorbents. J. Solid State Chem. 183, 2979–2986. https://doi.org/10.1016/j.jssc.2010.09.023.
Siswoyo, E., Mihara, Y., Tanaka, S., 2014. Determination of key components and adsorption capacity of a low cost adsorbent based on sludge of drinking water treatment plant to adsorb cadmium ion in water. Appl. Clay Sci. 97–98, 146–152. https://doi.org/10.1016/j.clay.2014.05.024.
Su, H., Wen, Y., Wang, F., Sun, Y., Tong, Z., 2008. Reductive leaching of manganese from low-grade manganese ore in H_2SO_4 using cane molasses as reductant. Hydrometallurgy 93, 136–139. https://doi.org/10.1016/j.hydromet.2008.01.001.
Su, Q., Pan, B., Pan, B., Zhang, Q., Zhang, W., Lv, L., Wang, X., Wu, J., Zhang, Q., 2009. Fabrication of polymer-supported nanosized hydrous manganese dioxide (HMO) for enhanced lead removal from waters. Sci. Total Environ. 407, 5471–5477. https://doi.org/10.1016/j.scitotenv.2009.06.045.
Sulaiman, R.N.R., Othman, N., 2017. Synergistic green extraction of nickel ions from electroplating waste via mixtures of chelating and organophosphorus carrier. J. Hazard Mater. 340, 77–84. https://doi.org/10.1016/j.jhazmat.2017.06.060.
Trifoni, M., Toro, L., Vegliò, F., 2001. Reductive leaching of manganiferous ores by glucose and H_2SO_4: effect of alcohols. Hydrometallurgy 59, 1–14. https://doi.org/10.1016/S0304-386X(00)00138-9.
Vaezi, F., Batebi, F., 2001. Recovery of iron coagulants from Tehran water-treatment-plant sludge for reusing in textile wastewater treatment. Iran. J. Public Health 30, 135–138.
Varma, R.S., Saini, R.K., Dahiya, R., 1997. Active manganese dioxide on silica: oxidation of alcohols under solvent- free conditions using microwaves. Tetrahedron Lett. 38, 7823–7824.
Villaseñor, J., Reyes, P., Pecchi, G., 2002. Catalytic and photocatalytic ozonation of phenol on MnO_2 supported catalysts. Catal. Today 76, 121–131. https://doi.org/10.1016/S0920-5861(02)00212-2.
Walanda, D.K., Lawrance, G.A., Donne, S.W., 2005. Hydrothermal MnO_2: synthesis, structure, morphology and discharge performance. J. Power Sources 139, 325–341. https://doi.org/10.1016/j.jpowsour.2004.06.062.
Xu, M., Liu, J., Hu, K., Xu, C., Fang, Y., 2016. Nickel(II) removal from water using silica-based hybrid adsorbents: fabrication and adsorption kinetics. Chin. J. Chem. Eng. 24, 1353–1359. https://doi.org/10.1016/j.cjche.2016.05.028.
Zhang, X., Wang, X., 2015. Adsorption and desorption of nickel(II) ions from aqueous solution by a lignocellulose/montmorillonite nanocomposite. PLoS One 10, 1–21. https://doi.org/10.1371/journal.pone.0117077.
Zhu, Q., Li, Z., 2015. Hydrogel-supported nanosized hydrous manganese dioxide: synthesis, characterization, and adsorption behavior study for Pb^{2+}, Cu^{2+}, Cd^{2+} and Ni^{2+} removal from water. Chem. Eng. J. 281, 69–80. https://doi.org/10.1016/j.cej.2015.06.068.